© 2018 IJSRST | Volume 4 | Issue 2 | Print ISSN: 2395-6011 | Online ISSN: 2395-602X
Themed Section: Science and Technology

Synthesis, Structural and Optical Properties of $Sr_3Y_2(BO_3)_4$: Tb^{3+} Phosphors

Sheetal*[1], Ritu Langyan[2], Sonika[1], S.P. Khatkar[1]
[1]Department of Chemistry, Maharshi Dayanand University, Rohtak, Haryana, India
[2]Department of Chemistry, Kurukshetra University, Kurukshetra, Haryana,India

ABSTRACT

Tb^{3+}-activated $Sr_3Y_2(BO_3)_4$ nanophosphors have been synthesized by combustion route using glycine as fuel and their photoluminescent properties have been investigated. Morphology and luminescent properties of $Sr_3Y_2(BO_3)_4$:Eu^{3+} nanoparticles were characterized by scanning electron microscopy, fluorescence spectrometry, and x-ray diffraction. The X-ray diffraction patterns (XRD) were used to investigate phase and crystal size of the prepared nanoparticles were found to have size between 20 to 40 nm. The emission spectra indicated the excellent green photoluminescent properties of $Sr_3Y_2(BO_3)_4$:Tb^{3+} nanoparticles due to characteristics transition of Tb^{3+} ions from $^5D_4 \rightarrow {}^7F_5$ at 545 nm. The dependence of the luminescence intensity on Tb^{3+} ions concentrations and effect of heat treatment have also been discussed.

Keywords: $Sr_3Y_2(BO_3)_4$:Tb^{3+}, Nanophosphor, Green luminescence, Crystal structure.

I. INTRODUCTION

Rare earth-doped $M_3Re_2(BO_3)_4$ crystal materials have been gained much interest [1-3]. As a member of this family, $Sr_3Y_2(BO_3)_4$ has been recently investigated as one of the best hosts for rare earth (RE) ions because of the large band-gap, easy synthesis, stability and low cost [4]. The hosts $Sr_3Y_2(BO_3)_4$ has orthorhombic structure with space group Pc21n and the lattice parameters are as follows: a=8.694Å, b=15.971Å, c=7.392Å, a=b=c=90° [5,6]. The structure of $Sr_3Y_2(BO_3)_4$ is formed by isolated BO_3 triangles, strontium–oxygen polyhedra, and yttrium–oxygen polyhedral. The Y^{3+} ion occupy two different crystallographic sites (Y1 and Y2) and each has an eightfold coordination to form YO_8 polyhedra. The bond valence of Y(1) is stronger than that of Y(2), so the Eu^{3+} prefers to occupy the Y(2) site. $Y(2)O_8$ polyhedra columns are built by sharing edges along the *c*-axis [4,7]. The structure of $Sr_3Y_2(BO_3)_4$ indicates that the longer distance between the rare-earth ions in the crystal structure of $Sr_3Y_2(BO_3)_4$ result in accommodation of higher doping concentration of the rare earth ion. As is well known, the efficient green emissions of Tb^{3+} originate from the magnetic dipole transition $^5D_4 \rightarrow {}^7F_5$ (545 nm). In the present work, glycine-assisted combustion synthesis technique has been exploited for the synthesis of $Sr_3Y_2(BO_3)_4$:Tb^{3+} phosphor. Various synthesis conditions such as temperature and terbium concentration have been varied in order to determine the exact optimal conditions for synthesizing these phosphors with superior optical properties.

II. MATERIAL AND METHODS

A. Powder Synthesis

$Sr_3Y_{2(1-x)}(BO_3)_4$:$2xTb^{3+}$ was synthesized by combustion method using high purity starting reagents $Sr(NO_3)_2$, $Y(NO_3)_3.6H_2O$, H_3BO_3, $Tb(NO_3)_3.6H_2O$ and glycine. The theoretical equation for the formation of these phosphors by combustion from metal nitrates and glycine at about 550°C may be shown as:

$3Sr(NO_3)_2 + 2(1-x)Y(NO_3)_3 + 4H_3BO_3 + 2xTb(NO_3)_3 + 10CH_4N_2O(glycine) \rightarrow Sr_3Y_{2(1-x)}Tb_{2x}(BO_3)_4$ + gaseous products.

According to nominal composition of $Sr_3Y_{2(1-x)}(BO_3)_4:2xTb^{3+}$ (x=0.01, 0.03, 0.05, 0.07 and 0.09), a stoichiometric amount of metal nitrates and boric acid were dissolved in minimum quantity of deionized water in 200 mL capacity pyrex beaker. Then glycine was added in this solution with molar ratio of glycine to oxidizer based on total oxidizing and reducing valencies of oxidizer and fuel (glycine) according to concept used in propellant chemistry [8]. Finally the beaker containing the solution was placed into a preheated furnace maintained at 550°C. The material undergoes rapid dehydration and foaming followed by decomposition, generating combustible gases. These volatile combustible gases ignite and burn with a flame yielding voluminous solid. The combustion process utilizes the enthalpy of combustion for the formation and crystallization of the phosphor at low ignition temperature. The powders obtained were calcined at different temperatures from 700°C to 1000°C for 3 h to increase the brightness.

B. Powder Characterization Techniques

Crystal phase of $Sr_3Y_2(BO_3)_4:Tb^{3+}$ powders were characterized by Rigaku Ultima-IV X-ray powder diffractometer with CuKα radiation to record the patterns in 2θ range of 10°-80°. Morphology and particle size were evaluated using Jeol JSM-6510 scanning electron microscope. Excitation and emission spectra of powders in the ultraviolet-visible region were obtained using Hitachi F-7000 fluorescence spectrophotometer with Xe- lamp as the excitation source. All the properties were investigated at room temperature.

III. RESULTS AND DISCUSSION

i. X-ray Diffraction Studies

The XRD patterns of $Sr_3Y_{1.86}Tb_{0.14}(BO_3)_4$ powders, as-prepared and calcined at different temperatures 700°C, 900°C and 1000°C for 3h are shown in fig.1.

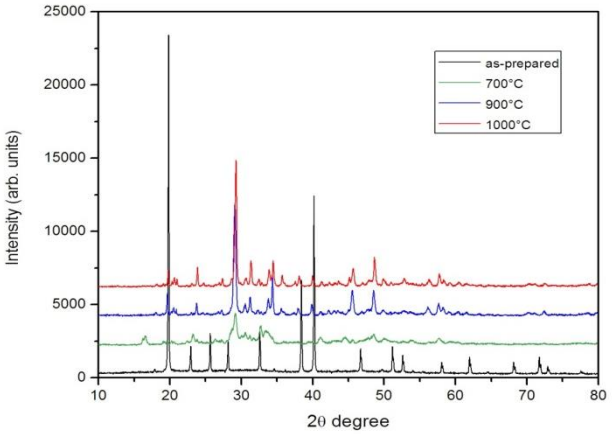

Figure 1. XRD patterns of $Sr_3Y_{1.86}Tb_{0.14}(BO_3)_4$ powders calcined at various temperatures.

XRD patterns of the as-prepared samples at 550°C show many additional peaks corresponding to those of unreacted $Sr(NO_3)_2$ phase (JCPDS card no. 04-0310) and $Y(NO_3)_3$ phase (JCPDS card no. 32-1487) respectively and no $Sr_3Y_2(BO_3)_4$ phase formation was observed. At further higher temperature of 700°C, the peaks characteristic due to $Sr_3Y_2(BO_3)_4$ phase appeared, while the peaks due to strontium nitrate and yttrium nitrate disappeared. At this temperature (700°C) the characteristic peak intensity at 2θ=29.263 was weak, but on further heating the sample at 900°C the enhancement of peak intensity is noticed. At 1000°C, a pure $Sr_3Y_2(BO_3)_4$ phase was obtained which matched well with literature data [7,9,10]. The diffraction peaks of $Sr_3Y_2(BO_3)_4$ can be indexed on the basis of a orthorhombic cell with the lattice parameters of a=0.87011 nm, b=1.59848 nm and c=0.73812 nm [11]. $Sr_3Y_2(BO_3)_4$ has an orthorhombic structure with Pc21n space group. No peaks from other phases can be detected at this temperature, indicating complete phase formation of the phosphor powder. The effect of Tb^{3+} ions doping on $Sr_3Y_2(BO_3)_4$ lattice seems to be

negligible as Tb^{3+} ions do not form new phases in the synthesis process.

The size of the crystallites can be estimated with the help of Scherrer equation, $D=0.94\lambda/\beta\cos\theta$, where D is the average crystallite size, λ is X-ray wavelength (0.15418 nm), θ is the diffraction angles and β is full-width at half-maximum (FWHM, in radian) of an observed peak, respectively [12]. The calculated average crystallite size (D) of $Sr_3Y_2(BO_3)_4:Tb^{3+}$ phosphor particles is found to be 20 nm at calcination temperature 700°C, 25 nm at calcination temperature 900°C and 32 nm at calcination temperatures of 1000°C. Hence, it can be concluded from the calculated results that with the increase of calcination temperature the crystallite size also becomes larger.

ii. Morphological Characteristics

Scanning electron microscope study is carried out to investigate surface morphology of the synthesized powders. SEM images of $Sr_3Y_{1.86}Tb_{0.14}(BO_3)_4$ phosphors, as-synthesized and calcined at 700°C, 900°C and 1000°C are displayed in fig. 2(a-d). The as-synthesized product depicts unusual morphology i.e. cracks, voids and porous network as shown in fig. 2(a). This is due to escaping gases during combustion process. The SEM micrograph shown in fig. 2(b) reveals that the morphology of the sample calcined at 700°C has small and coagulated particles with almost amorphous phase having small size distribution. The phosphor particles grow to sphere shape with further rise of temperature to 900°C. Fig. 2(d) displays the smooth and spherical particles of terbium doped phosphors calcined at 1000°C. The particle size increased as expected from temperature 700°C to 1000°C. Also the phenomenon of agglomeration is found to decrease at higher temperatures.

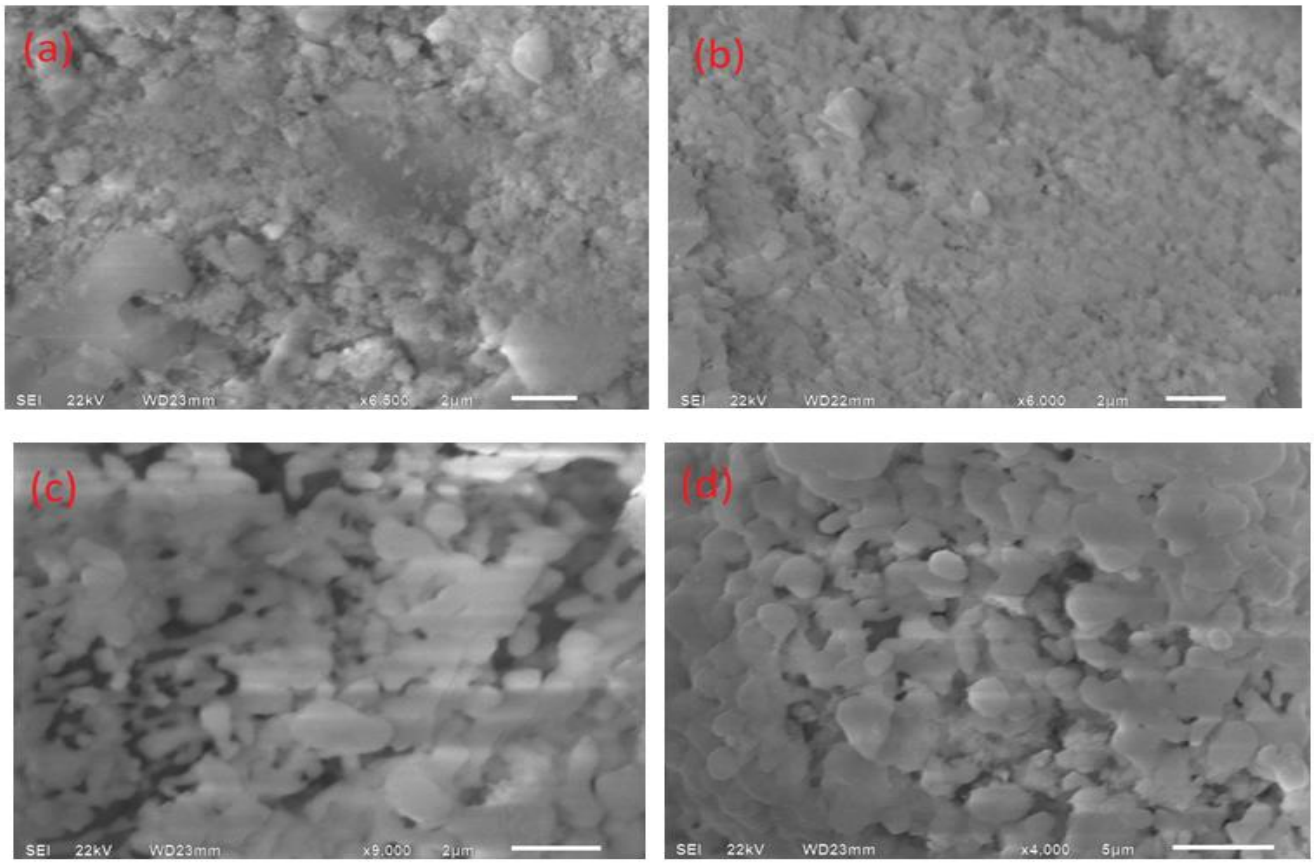

Figure 2. SEM micrographs of $Sr_3Y_{1.86}Tb_{0.14}(BO_3)_4$ (a) as-synthesized; calcined at (b) 700°C (c) 900°C and (d) 1000°C temperatures.

iii. Luminescent Properties

Figure 3 shows the excitation spectrum of $Sr_3Y_{1.86}Tb_{0.14}(BO_3)_4$ calcined at 1000° C, λ_{em}=545 nm. The excitation spectrum consists of a broad band in the range from 200 nm to 280 nm with a maximum at about 243 nm and a series of sharp peaks between 300 nm to 500 nm with very low intensity. The high intensity band at 243 nm is assigned to spin-allowed $4f^8$–$4f^75d^1$ transitions of Tb^{3+} ions in the $Sr_3Y_2(BO_3)_4$ host lattice. The peaks in the longer wavelength region beyond 300 nm are assigned to Tb^{3+} intra-4f transitions ($4f^8$–$4f^8$) from the ground state to higher energy levels. The dominant excitation peaks at 320 nm, 340 nm, 352 nm, 369 nm, 379 nm and 485 nm can be attributed to $^7F_6 \rightarrow {}^5D_1$, $^7F_6 \rightarrow {}^5L_7$, $^7F_6 \rightarrow {}^5D_2$, $^7F_6 \rightarrow {}^5D_3$, $^7F_6 \rightarrow {}^5L_{10}$ and $^7F_6 \rightarrow {}^5D_4$ transitions of Tb^{3+} respectively [13,14].

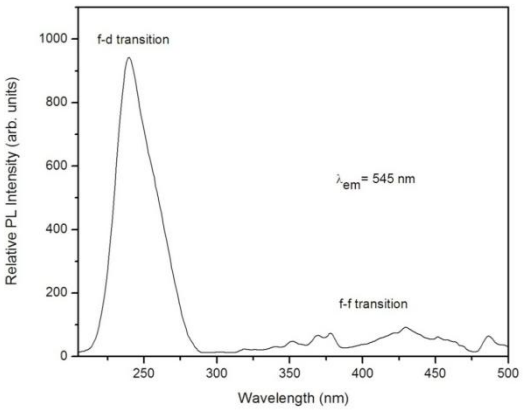

Figure 3. Excitation spectrum of $Sr_3Y_{1.86}Tb_{0.14}(BO_3)_4$ sample calcined at 1000°C, λ_{em}=545 nm.

The emission spectra of $Sr_3Y_2(BO_3)_4:Tb^{3+}$ under excitation wavelength of 243 nm are shown in fig. 4. The emission spectra of $Sr_3Y_2(BO_3)_4:Tb^{3+}$ comprises of stronger peaks due to Tb^{3+} transitions $^5D_4 \rightarrow {}^7F_6$, $^5D_4 \rightarrow {}^7F_5$, $^5D_4 \rightarrow {}^7F_4$ and $^5D_4 \rightarrow {}^7F_6$ at emission wavelengths 489 nm, 545 nm, 584 nm and 622 nm respectively [15,16]. The magnetic dipole transition $^5D_4 \rightarrow {}^7F_5$ (545 nm) is dominant resulting in green emission of the phosphor. The relative photoluminescent intensity of $Sr_3Y_{1.86}Tb_{0.14}(BO_3)_4$ as a function of temperature, at λ_{ex}=243 nm is shown in fig. 4(a). The photoluminescence intensity of the phosphor is found to increase with increase in calcination temperature. The intensity is found to be maximum for the sample calcined at 1000°C. These observations can be explained by the fact that crystallinity increases with increase in temperature. The luminescence intensities of the phosphor are dependent on the dopant concentration. Fig. 4(b) displays dependence of PL intensity of $Sr_3Y_2(BO_3)_4:Tb^{3+}$ on the concentration of dopant Tb^{3+}. It is quite clear that PL intensity of $Sr_3Y_{2(1-x)}(BO_3)_4:2xTb^{3+}$ (x=0.01-0.09) increases with increasing Tb^{3+} concentration, reaching a maximum value at x=0.07 and thereafter decreases with further increase in Tb^{3+} concentration due to mutual Tb^{3+}-Tb^{3+} interactions.

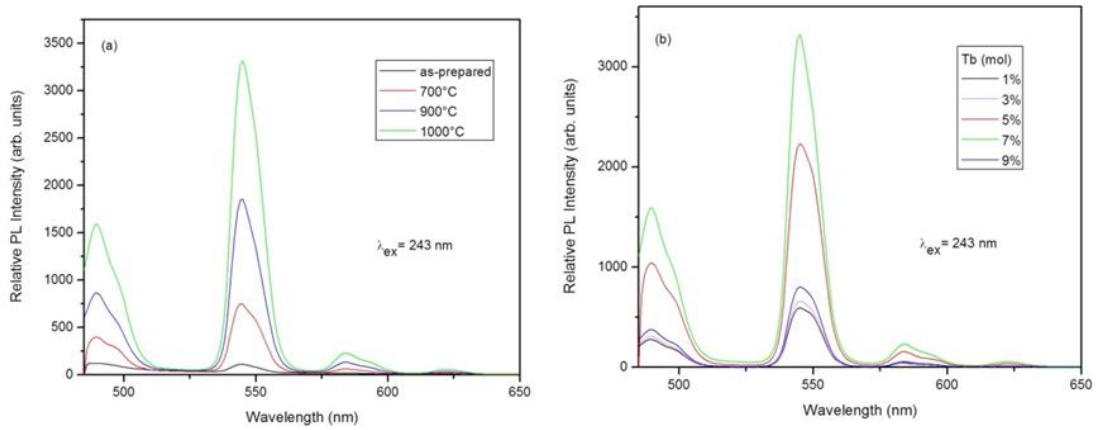

Figure 4. (a) Emission spectra of $Sr_3Y_{1.86}Tb_{0.14}(BO_3)_4$ showing relative photoluminescent intensity as a function of temperature and (b) Emission spectra of $Sr_3Y_{2(1-x)}(BO_3)_4:2xTb^{3+}$ (x=0.01, 0.03, 0.05, 0.07 and 0.09) showing variation of emission intensity as a function of Tb^{3+} concentrations, λ_{ex}=243 nm.

IV. CONCLUSION

$Sr_3Y_2(BO_3)_4:Tb^{3+}$ was prepared at 550°C by combustion method using glycine as an organic fuel. The solid obtained was again calcined at 700°C to 1000°C for 3 h to increase the brightness. XRD analysis reveals that a pure orthorhombic structure $Sr_3Y_2(BO_3)_4$ phase was obtained at 1000°C. SEM image of as-synthesized product shows cracks, voids and porous network due to escaping gases during combustion. On increasing temperature smooth and spherical particles are obtained. The average grain size is less than 1μm. The particle size increased and agglomeration is found to decrease from temperature 700°C to 1000°C. The optimum concentration of Tb^{3+} was found to be 7 mol% in the host lattice. The main emission peak located at 545 nm was observed from magnetic dipole transition $^5D_4 \rightarrow {}^7F_5$ of Tb^{3+} at λ_{ex}=243 nm.

V. REFERENCES

[1]. B. Wei, Z.S. Hu, Z.B. Lin, L.Z. Zhang, G.F. Wang, J. Cryst. Growth, 273 (2004) 190.

[2]. Y. Zhang, Z.B. Lin, Z.S. Hu, G.F. Wang, J. Cryst. Growth, 177 (2004) 3184.

[3]. P.-H. Haumesser, R. Gaume, J.-M. Benitez, B. Viana, B. Ferrand, G. Aka, D. Vivien, J. Cryst. Growth, 233 (2001) 233.

[4]. Y. Zhang, Y. Li, J. Alloys Compd., 384 (2004) 88.

[5]. Q. Wei, X.Z. Li, G. Wang, M. Song, Z. Wang, G. Wang, X. Long, Opt. Mater., 30 (2008) 1495.

[6]. Z. Rui, W. Xiang, J. Alloys Compd., 509 (2011) 1197.

[7]. L. He, Y. Wang, J. Alloys Compd., 431 (2007) 226.

[8]. S. Ekambaram, K.C. Patil, J. Alloys Compd., 448 (1997) 7.

[9]. P. Li, Z. Yang, Z. Wang, Q. Guo, Mater. Lett., 62 (2008) 1455.

[10]. P. Li, Z. Yang, Z. Wang, Q. Guo, Chin. Phys. B, 17 (2008) 1907.

[11]. A. Boultif, D. Louer, J. Appl. Crystallogr., 24 (1991) 987.

[12]. X.Q. Zeng, G.Y. Hong, H.P. You, X.Y. Wu, Chin. J. Lumin., 22 (2001) 58.

[13]. Y. Yang, A. Bao, H. Lai, Y. Tao, H. Yang, J. Phys. Chem. Solids, 70 (2009) 1317.

[14]. G. Li, Y. Lai, W. Bao, L. Li, M. Li, S. Gan, T. Long, L. Zou, Powder Technol., 214 (2011) 211.

[15]. Z.J. Zhang, J.L. Yuan, H.H. Chen, X.X. Yang, J.T. Zhao, G.B. Zhang, C.S. Shi, Solid State Sci., 11 (2009) 549.

[16]. U. Rambabu, D.P. Amalnerkar , B.B. Kale, S. Buddhudu, Mater. Chem. Phys., 70 (2001) 1.